



## Research Paper

# Stoichiometric quantification of the thiol redox proteome of macrophages reveals subcellular compartmentalization and susceptibility to oxidative perturbations

Jicheng Duan<sup>a,1</sup>, Tong Zhang<sup>a,1</sup>, Matthew J. Gaffrey<sup>a</sup>, Karl K. Weitz<sup>a</sup>, Ronald J. Moore<sup>a</sup>, Xiaolu Li<sup>c</sup>, Ming Xian<sup>b</sup>, Brian D. Thrall<sup>a</sup>, Wei-Jun Qian<sup>a,\*</sup>

<sup>a</sup> Biological Sciences Division, Pacific Northwest National Laboratory, Richland, WA, USA

<sup>b</sup> Department of Chemistry, Washington State University, Pullman, WA, USA

<sup>c</sup> Department of Biological Systems Engineering, Washington State University, Richland, WA, USA



## ARTICLE INFO

## Keywords:

Protein thiols  
Redox modification  
Redox proteomics  
S-glutathionylation  
Site-occupancy  
Stoichiometry  
Macrophages  
Resin-assisted capture  
RAC-TMT

## ABSTRACT

Posttranslational modifications of protein cysteine thiols play a significant role in redox regulation and the pathogenesis of human diseases. Herein, we report the characterization of the cellular redox landscape in terms of quantitative, site-specific occupancies of both S-glutathionylation (SSG) and total reversible thiol oxidation (total oxidation) in RAW 264.7 macrophage cells under basal conditions. The occupancies of thiol modifications for ~4000 cysteine sites were quantified, revealing a mean site occupancy of 4.0% for SSG and 11.9% for total oxidation, respectively. Correlations between site occupancies and structural features such as pKa, relative residue surface accessibility, and hydrophobicity were observed. Proteome-wide site occupancy analysis revealed that the average occupancies of SSG and total oxidation in specific cellular compartments correlate well with the expected redox potentials of respective organelles in macrophages, consistent with the notion of redox compartmentalization. The lowest average occupancies were observed in more reducing organelles such as the mitochondria (non-membrane) and nucleus, while the highest average occupancies were found in more oxidizing organelles such as endoplasmic reticulum (ER) and lysosome. Furthermore, a pattern of subcellular susceptibility to redox changes was observed under oxidative stress induced by exposure to engineered metal oxide nanoparticles. Peroxisome, ER, and mitochondria (membrane) are the organelles which exhibit the most significant redox changes; while mitochondria (non-membrane) and Golgi were observed as the organelles being most resistant to oxidative stress. Finally, it was observed that Cys residues at enzymatic active sites generally had a higher level of occupancy compared to non-active Cys residues within the same proteins, suggesting site occupancy as a potential indicator of protein functional sites. The raw data are available via ProteomeXchange with identifier PXD019913.

## 1. Introduction

Cellular redox homeostasis, maintained by continuous signaling for the production and elimination of electrophiles and nucleophiles, is an essential feature of a healthy physiological steady state, whereas a shift from the redox homeostasis is often associated with pathological conditions [1]. Changes in the cellular redox state may trigger reversible redox-dependent posttranslational modifications (redox PTMs) on protein thiols including disulfide formation, S-glutathionylation (SSG), S-sulfonylation (SOH), S-nitrosylation (SNO), and S-sulphydration (SSH)

[2,3]. By switching between the oxidized and reduced forms, these redox PTMs could lead to significant biological consequences such as gain/loss of enzymatic activity, change of subcellular location, and enhanced/decreased interactions with other molecules, which further impact down-stream biological responses to redox signals [4,5]. Aberrant redox signaling has been implicated in many human diseases such as cancer, diabetes, and other aging-related diseases [6–10]. In addition, the role of specific redox modifications such as SSG has also been recognized as a potential signaling and regulatory paradigm linking reactive oxygen species (ROS)-mediated oxidative stress and diseases [11–13]. Quantitative measurements of the thiol redox proteome at both

\* Corresponding author. PO Box 999, MSIN K8-98, Biological Science Division, Pacific Northwest National Laboratory, Richland, WA, 99352, USA.

E-mail address: [weijun.qian@pnl.gov](mailto:weijun.qian@pnl.gov) (W.-J. Qian).

<sup>1</sup> These authors contribute to this work equally.

<https://doi.org/10.1016/j.redox.2020.101649>

Received 27 May 2020; Received in revised form 24 June 2020; Accepted 17 July 2020

Available online 21 July 2020

2213-2317/© 2020 The Authors.

Published by Elsevier B.V. This is an open access article under the CC BY-NC-ND license

(<http://creativecommons.org/licenses/by-nc-nd/4.0/>).

**Abbreviations**

Cys	cysteine
CV	coefficient of variation
DTT	dithiothreitol
ENP	engineered nanoparticles
ER	endoplasmic reticulum
GO	gene ontology
GSH	glutathione
GSSG	oxidized glutathione
NEM	<i>N</i> -ethylmaleimide
NP	nanoparticle
RAC	resin-assisted capture
RAC-TMT	resin-assisted capture coupled with TMT labeling
ROS	reactive oxygen species
RSA	relative residue surface accessibility
SNO	S-nitrosylation
SOH	S-sulfonylation
SSG	S-glutathionylation
SSH	S-sulfhydration
TMT	tandem mass tag

the basal state and under oxidative stress conditions are critical for a detailed understanding of redox regulation in signaling and pathogenesis.

Mass spectrometry (MS)-based redox proteomics is an emerging tool for characterizing the thiol redox proteome and its role in redox signaling and regulation [2,14–16]. In particular, proteome-wide site-specific quantification of redox PTMs has provided a landscape view of cellular redox signaling networks [14,15,17]. As a result, thousands of redox sensitive Cys sites have been documented in a number of databases, providing an invaluable resource for redox biology [18–20]. The analytical power of MS-based redox proteomics has also been harnessed to compare the relative thiol oxidation levels among different experimental groups [21,22]. In addition to relative fold changes among different conditions, accurate quantification of site occupancy or stoichiometry of specific redox PTMs is also critical for understanding the biological significance of individual Cys residues as well as the overall cellular redox status. The site-specific PTM occupancy data in combination with redox sensitivity (i.e., fold change) were shown to provide predictive values for delineating functionality of individual Cys sites [23–25].

Given the significance of PTM occupancies, a number of studies have attempted to perform such measurements for the occupancies of either total thiol oxidation or specific types of redox PTMs in various organisms using redox proteomics [26–33]. We have reported a multiplexed quantitative redox proteomics approach that integrates resin-assisted capture with multiplexed isobaric TMT (tandem mass tag) labeling (RAC-TMT), and high resolution LC-MS/MS for proteome-wide site-specific quantification profiling of thiol-based redox PTMs [21,31,34–36]. Using this approach, we have demonstrated the regulatory roles of SSG in macrophages during metal oxide engineered nanoparticle (ENP)-induced oxidative stress, supporting the importance of redox regulation in immune function [21]. However, a broad characterization of site occupancy of redox PTMs of the thiol proteome in macrophages has not been reported. Measurements under basal conditions would provide a detailed cellular landscape view and a baseline of thiol redox state, upon which site-specific redox sensitivity can be determined by integrating data from perturbations.

In this work, we aim to characterize the basal thiol redox proteome of mouse RAW macrophages by simultaneous quantification of the site occupancies of SSG and total oxidation in unstimulated cells. Macrophages are the first line of defense for the clearance of pathogens and

other foreign materials, playing a pivotal role in the innate immune response. The involvement of SSG in mediating several key macrophage processes such as cytoskeletal remodeling, cell migration, and cell signaling had been well documented [37–39]. Using our redox proteomics approach, we characterized the basal levels of SSG and total oxidation for more than 4000 Cys residues in macrophages. The broad distributions and large dynamic ranges of site-specific PTM occupancies provided insights into the complexity of redox regulatory networks. Bioinformatics analysis further revealed distinct patterns of cellular redox compartmentalization based on the average levels of site occupancies for proteins in individual subcellular compartments. Moreover, subsequent integration of data on relative changes induced by oxidative stress revealed differences in susceptibility to oxidative stress across different compartments. These measurements of the basal thiol redox proteome provides interesting details of macrophage physiology with regard to the redox landscape, subcellular redox compartmentalization and susceptibility towards oxidative stress.

## 2. Materials and methods

### 2.1. Cell culture, lysis, free thiol blocking, and protein extraction

Mouse macrophages (RAW 264.7, ATCC # TIB 71) were cultured in RPMI 1640 supplemented with 10% FBS, 2 mM L-glutamine (Fisher Scientific, Rockford, IL), and 1% penicillin–streptomycin (Fisher Scientific, Rockford, IL). Cells were kept in an incubator at 37 °C with 5% CO<sub>2</sub>. For lysis, cells were rinsed twice with RPMI-1640 without supplements and harvested in lysis buffer (250 mM HEPES, 1% Triton X-100, pH 7.0). Freshly prepared 100 mM *N*-ethylmaleimide (NEM) (Fisher Scientific, Rockford, IL) was included for the SSG and total oxidation samples, but not for total thiol samples. Cell lysates were centrifuged at 14,000 rpm for 10 min at 4 °C and the soluble protein fraction was retained. NEM-alkylation was carried out at 55 °C in dark for 30 min, followed by acetone precipitation for overnight at –20 °C. Protein pellets were re-suspended in 250 mM HEPES containing 8 M urea (pH 7.5) and 0.1% SDS, followed by buffer exchange to 25 mM HEPES containing 1 M urea (pH 7.5) by using 0.5 mL Amicon Ultra 10 K filter units (EMD Millipore, MA). Protein concentration was determined by using the bicinchoninic acid assay (BCA).

### 2.2. Resin-assisted capture of protein thiols, on-resin tryptic digestion, and TMT labeling

For the reduction of SSG-modified proteins, 480 µg of the NEM-blocked samples were diluted to 1 µg/µL with 25 mM HEPES containing 1 M urea (pH 7.5), followed by the addition of 2.5 µg/mL Glutaredoxin Grx1M (C14S mutant from *E. coli*, IMCO Corp. Ltd. AB), 0.25 mM oxidized glutathione (GSSG), 1 mM NADPH, and 4 U/mL Glutathione Reductase (GR). Samples were incubated at 37 °C for 10 min, immediately placed on ice and transferred to a 0.5 mL Amicon Ultra 10 K filter. Excess reagents were removed by buffer exchanged with 3 × 8 M urea (pH 7.0) resulting in a final volume of 30–40 µL. Protein concentration of the de-glutathionylated samples was measured by the BCA assay before enrichment. Similar procedures were followed for the total oxidation and total thiol samples, except that the reduction reaction was performed with 20 mM dithiothreitol (DTT) at 37 °C for 30 min.

For enrichment, 350 µg of the reduced samples were resuspended in 120 µL of 25 mM HEPES buffer (pH 7.7) containing 0.2% SDS and loaded to spin columns (Thermo Scientific, Waltham, MA) containing 30 mg pre-conditioned Thiopropyl Sepharose 6B resin. Enrichment was carried out in a thermomixer at room temperature with shaking at 850 rpm for 2 h. The experimental conditions for resin washing, on-resin tryptic digestion and tandem mass tag (TMT) labeling, DTT elution and C18 cleanup were performed as previously described [21,36,40]. The enriched peptides were dissolved in a final volume of 30 µL H<sub>2</sub>O containing 20 mM DTT prior to liquid chromatography–tandem mass

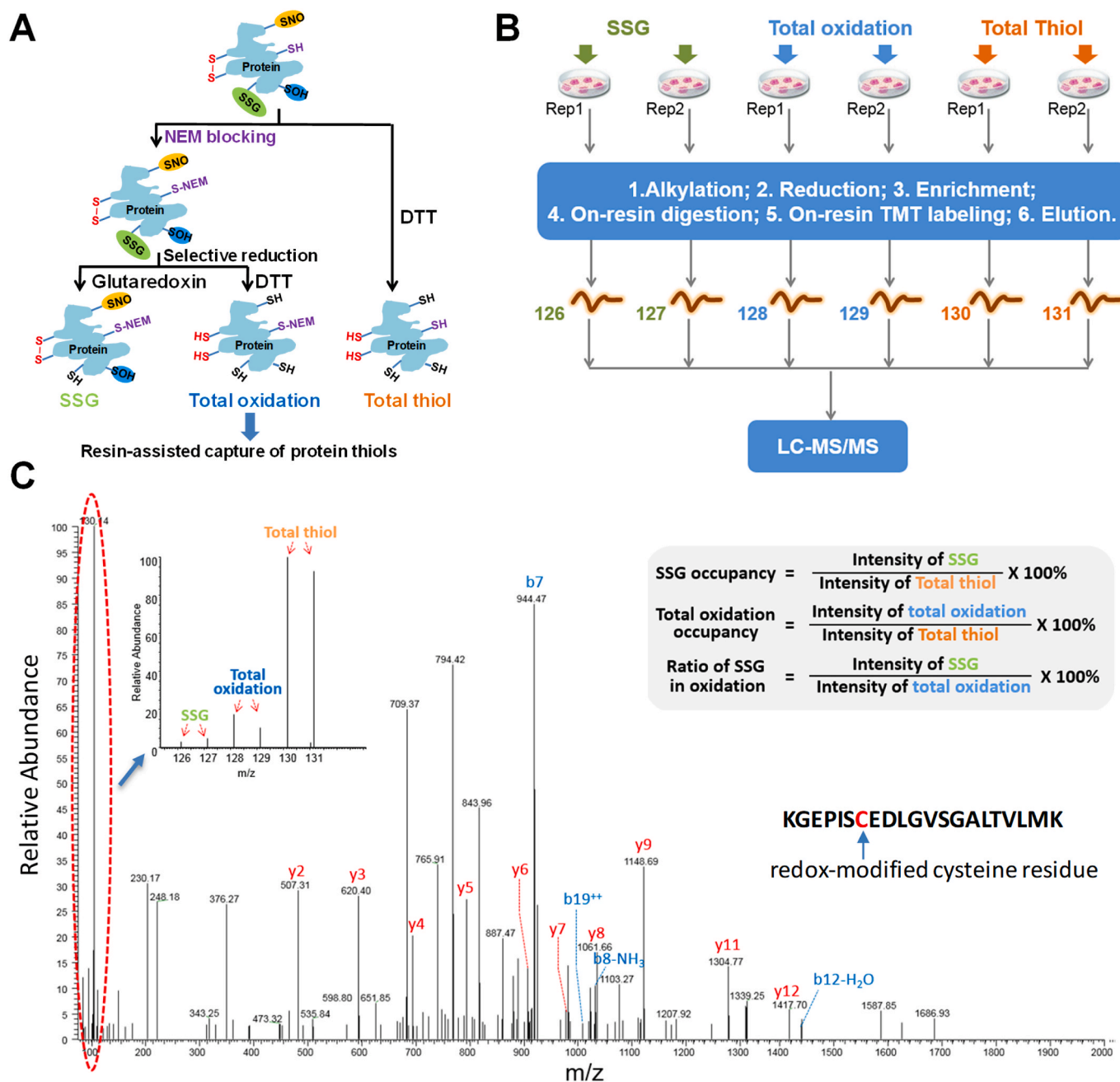


**Fig. 1.** Scheme for occupancy analysis of multiple redox modifications. (A) Protein samples were aliquoted into three equal parts to determine the levels of three redox modifications simultaneously: SSG, total oxidation (reversible oxidation such as SSG, SNO, SOH and SSH modifications), and total thiol (total oxidation plus free thiol in the reduced status initially). NEM blocking is performed for SSG and total oxidation samples, but skipped for total thiol samples. After blocking, SSG and total oxidation samples are selectively reduced by glutaredoxin and DTT, respectively. The total thiol samples are reduced by DTT. Newly generated thiols are subjected for enrichment. (B) Multiplexing of quantification is enabled by TMT6plex, where two replicates of each modification can be analyzed in a single LC-MS run. (C) A representative MS/MS spectrum to show peptide identification and determination of site occupancy.

spectrometry (LC-MS/MS) analysis.

### 2.3. LC-MS/MS

LC-MS/MS was performed as previously described [21]. Briefly, MS analysis was performed on a Thermo Scientific LTQ-Orbitrap Velos Pro mass spectrometer (Thermo Scientific, San Jose, CA) coupled with an electrospray ionization interface using a home-made 150 μm o.d. × 20 μm i.d. chemically etched electrospray emitter. The heated capillary temperature and spray voltage were 350 °C and 2.2 kV, respectively. Full MS spectra were recorded at resolution of 60 K over the range of *m/z*

300–2000 with an automated gain control (AGC) value of  $1 \times 10^6$ . MS/MS was performed in data-dependent mode at a resolution of 7.5 K with an AGC target value of  $3 \times 10^4$ . The most abundant 10 parent ions were selected for MS/MS using high-energy collision dissociation (HCD) with a normalized collision energy setting of 45. Precursor ion activation was performed with an isolation width of 2.5 Da, a minimal intensity of 1000 counts, and an activation time of 0.1 s. A dynamic exclusion time of 60 s was used.

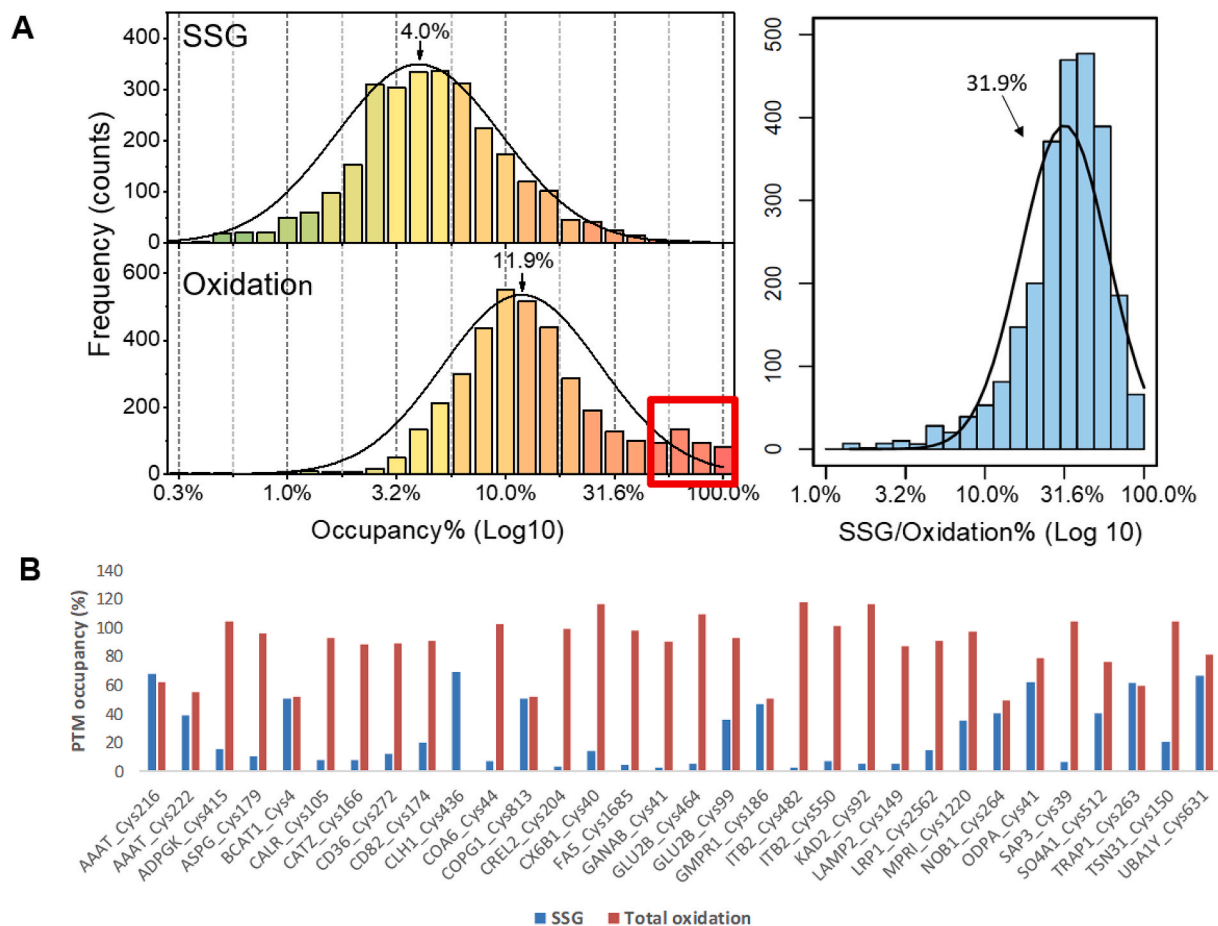


**Fig. 2.** Distribution of redox modification occupancy under physiological conditions. (A) The occupancy for both SSG (upper left, averages around 4.0%) and total oxidation (lower left, averages around 11.9%) spans a broad range, and SSG is a major form of reversible redox modifications constituting 31.9% of total oxidation on average (right). (B) PTM occupancies for selected protein Cys sites that displayed high occupancy of total oxidation.

#### 2.4. Data analysis

LC-MS/MS raw data were converted into dta files using Bioworks Cluster 3.2 (Thermo Fisher Scientific, Cambridge, MA), and the MS-GF+ algorithm [41] (v9979, released in March 2014) was used to search MS/MS spectra against the mouse protein sequence database (UniProt, released in September 2013). Key search parameters used were 20 ppm tolerance for precursor ion masses, 0.5 Da tolerance for fragment ions, partial tryptic search with up to 2 missed cleavages, dynamic oxidation of methionine (15.9949 Da), dynamic NEM modification of Cys (125.0477 Da), and static 6-plex TMT modification of lysine and N-termini of peptides (229.1629 Da). Peptides were identified from database searching results applying the following criteria: MSGF E-value  $< 10^{-10}$ , Q-value  $< 0.01$ , and mass measurement error  $< 10$  ppm ( $\pm 5$  ppm). The decoy database searching methodology [42] was used to confirm the final false discovery rate at the unique peptide level to be  $\sim 0.9\%$ . Since NEM blocked original free Cys sites, all glutathionylated Cys residues were identified as un-modified Cys.

For TMT-based relative quantification, all MS/MS spectra were grouped based on individual Cys-sites. The intensity of TMT reporter ion was summed from all spectra corresponding to a given Cys-site. Site occupancy was calculated as the average intensities of SSG or total oxidation divided by average intensities of total thiols, respectively. Several steps were conducted to ensure measurement quality. Firstly, Cys sites with less than two biological replicates in quantification were removed. Second, measurements with high coefficient of variation (CV) across replicates (1.5 standard deviation above the median CV) was considered as unreliable and were filtered out [43]. The average CV of

these measurements was  $\sim 13\%$  (Supporting Data 1).

Gene Ontology (GO) was performed using DAVID (<https://david.nci.crf.gov/>) [44]. The enriched GO terms were further processed by REVIGO (<http://revigo.irb.hr/>) to remove redundancy and then clustered using z-scores that are transformed from enrichment analysis p-values. Protein motif analysis was carried out using MOTIF tools ([www.genome.jp/tools/motif](http://www.genome.jp/tools/motif)). For functional annotation, several PTM databases were used, including dbGSH [18] (Cys S-glutathionylation database with 2006 SSG-modified Cys sites from 1128 proteins), dbSNO [45] (Cys S-nitrosylation database with 2646 SNO-modified Cys sites from 1355 proteins) and protein disulfide database from UniProt (<http://www.uniprot.org>, annotation for 29782 Cys sites from 2867 proteins).

The prediction of pKa values for Cys residues were carried out with PROPKA software by using available crystal structures of proteins from Protein Data Bank (PDB) database as input [46]. The relative solvent accessibility (RSA) for all Cys residues was calculated using NetSurf [47]. Subcellular localization annotation was based on the MetazSecKB Database (<http://bioinformatics.yu.edu/secretomes/animal/index.php>) [48].

#### 2.5. Data availability

The mass spectrometry proteomics data have been deposited to the ProteomeXchange Consortium via the PRIDE partner repository with the dataset identifier PXD019913 and 10.6019/PXD019913.

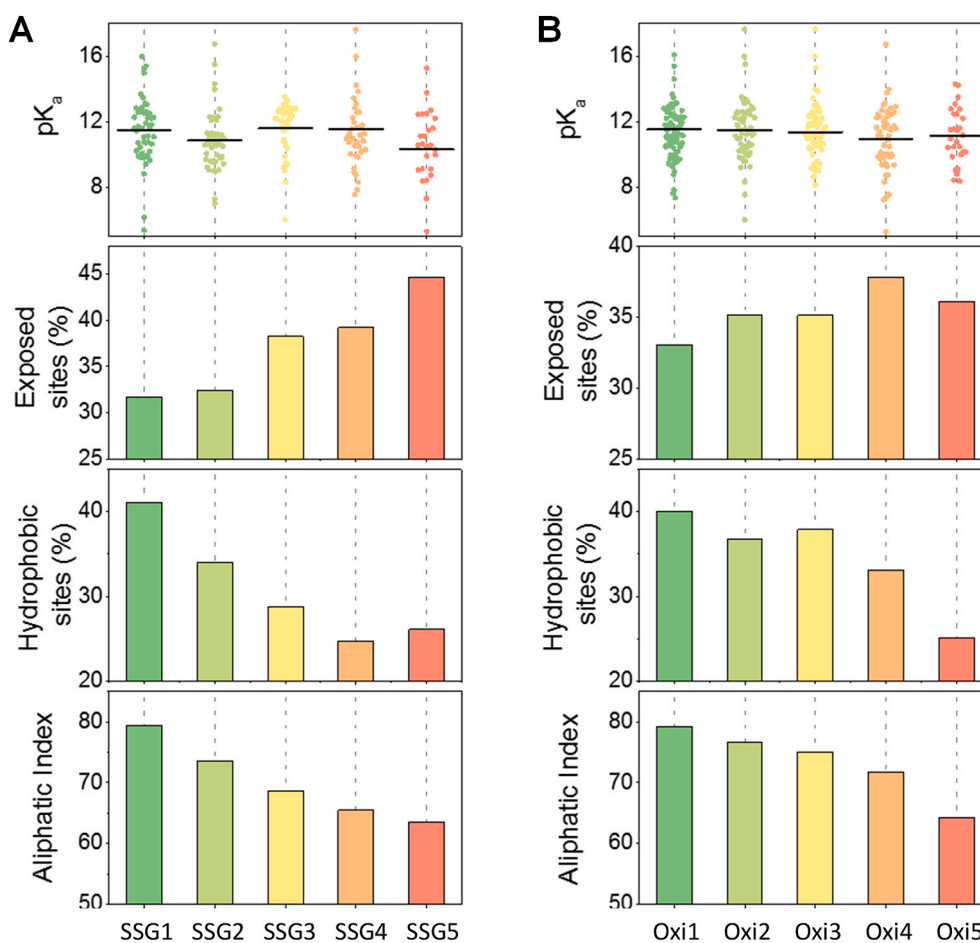


**Fig. 3.** Correlation between the structural properties and site occupancies of redox PTMs. The average pKa, exposed surface area, hydrophobicity, and aliphatic index of cysteine sites in each subgroup of SSG (A) and total oxidation (B) were plotted separately.

### 3. Results

#### 3.1. Proteome-wide measurements of site occupancies of SSG and total oxidation

Fig. 1 illustrates the experimental workflow for characterizing the PTM occupancies of SSG and total oxidation in mouse RAW macrophages under basal physiological conditions. Briefly, the workflow consists of three main steps: 1) initial blocking of free Cys thiols by NEM, 2) selective reduction of reversibly oxidized Cys residues, and 3) resin-assisted capture of the nascent protein thiols (Fig. 1A). Cell lysate from each replicate was first divided into three identical aliquots, which were processed separately for quantifying SSG, total oxidation, and total thiol, respectively, by using the multiplexed TMT labeling strategy (Fig. 1B). NEM blocking was performed only for SSG and total oxidation samples, but not for total thiol samples. Selective reduction of SSG samples was conducted with an enzyme cocktail containing a mutant form of GRX1 as previously described [21]. DTT was used to reduce all reversibly oxidized protein thiols in both the total oxidation and total thiol samples [36,40]. After reduction, free thiol-containing proteins were captured by Thiopropyl Sepharose 6B resin, followed by on-resin trypsin digestion and TMT labeling. The 6-plex TMT reagents allowed us to quantify SSG, total oxidation, and total thiols for two biological replicates in a single LC-MS/MS run (Fig. 1B). Two independent 6-plex TMT experiments were conducted to provide a total of four biological replicates for quantitative analysis. In total, 5684 Cys sites from 2347 proteins were identified and the specificity of the resin-assisted enrichment, as determined as the percentage of Cys-containing peptides over

all peptides detected, was 97%. Fig. 1C shows a representative MS/MS spectrum of a Cys-containing peptide where the TMT reporter ions in the low  $m/z$  region provide the intensity information for SSG, total oxidation and total thiol, respectively.

The site occupancies of SSG and total oxidation on a given Cys residue can be calculated as the percentage of the TMT reporter ion intensities for SSG and total oxidation *versus* the intensity for total thiol, respectively (Fig. 1C). The total oxidation herein refers to all reversible thiol modifications. Irreversible oxidation products such as  $-\text{SO}_2\text{H}$  and  $-\text{SO}_3\text{H}$  were not considered in this approach; however, the abundances of these forms under normal physiological conditions are likely negligible for most Cys sites [49]. Thus, the site occupancy for total oxidation reported here is an estimate of all reversible cysteine modifications such as disulfide, SSG, SNO and SOH. This strategy also allowed us to assess the ratio of SSG over total oxidation as the percentage of report ion intensities for SSG *versus* total oxidation.

Following stringent criteria for quantitative analysis (see Methods), we confidently determined the occupancies for 4099 Cys sites from 1959 unique proteins (Supporting Data 1). The site occupancy data were then log10 transformed so that the percent occupancy data can be displayed evenly across the logarithmic scale. Fig. 2A illustrates the bell-shaped histograms for SSG and total oxidation occupancies as well as SSG/total oxidation ratios in percentages. The occupancies of SSG and total oxidation span more than three orders of magnitude ranging from 0.01% to 69.1% and 0.6%–100%, respectively, which is consistent with the notion that Cys oxidation is highly dynamic, heterogeneous, and site-dependent in nature [5]. The average levels of cellular protein SSG and total oxidation were  $\sim 4.0\%$  and  $11.9\%$ , respectively, in good

agreement with prior reports that protein thiols are mostly in a reduced state *in vivo* [26,50]. The observed ~4.0% SSG occupancy is also consistent with ~4.5% SSG occupancy we recently observed in the mouse muscle proteome [31]. Moreover, the percentage of SSG over total oxidation is from 0.63% to 100% with a mean value of 31.9% (Fig. 2A), supporting that SSG is a major type of thiol-based redox PTMs [13] and that other forms of oxidative modifications could co-exist on the same Cys residues.

There is a significant portion of Cys sites that displayed high occupancies of total oxidation (>50%) (highlighted in Fig. 2A); however, most of these sites had relatively low SSG occupancies (mean occupancy ~13%). Most of the proteins with these high occupancy Cys sites (selected examples shown in Fig. 2B) are localized in the ER, lysosome, Golgi apparatus, or extracellular/membrane domain, suggesting that disulfide formation may be a primary mechanism for the high oxidation occupancies for these Cys sites. Indeed, nearly 60% of these highly oxidized Cys sites were annotated as sites containing disulfides in UniProt knowledgebase. Furthermore, the observations of low levels of SSG in Cys sites with high total oxidation occupancies not only support that the SSG protocol has a good specificity in selective reduction of SSG instead of protein disulfide, but also suggest that SSG and disulfide formation occur through distinct mechanisms.

Cys sites were further sorted and divided into five subgroups based on their occupancy levels ranging from low to high. The 20th, 40th, 60th and 80th percentiles were chosen as the boundaries among subgroups (Table S1). We then mapped the identified Cys sites (Fig. S1) against several existing redox databases (dbSNO, dbGSH and disulfide database) where redox-sensitive Cys sites have been compiled [18–20]. In general, the low occupancy groups (SSG1, SSG2, Oxi1, Oxi2) had a much higher matching in both dbSNO and dbGSH, while high occupancy sites (SSG5 or Oxi5) had a higher matching rate in the disulfide database (Fig. S1 B and D). The results are not surprising in that high occupancy sites at basal condition are more likely to be the result of disulfides while the low-occupancy residues (more reduced) at basal level are likely to be sensitive to redox signals, leading to SNO and SSG formation under oxidative stress.

### 3.2. Structural features of Cys residues with different levels of occupancies

To explore potential structural features of Cys residues, we carried out an in-depth structural and biochemical analysis. Specifically, we determined the correlations between the site occupancy and the following structural features: (i) pKa value, (ii) relative residue surface accessibility (RSA), (iii) hydrophobicity by GRAVY score [51], and (iv) stability by Aliphatic index [52].

The pKa value of protein thiol is known to be closely associated with its reactivity. Cys residues with low pKa values are often reactive at physiological pH [53]. The average pKa values of Cys residues were compared among subgroups. As shown in Fig. 3A, Cys sites with the highest SSG occupancy (SSG5) had an average pKa value about 0.5–1.3 pH units lower than those in the other SSG subgroups. However, the difference among subgroups were not statistically significant ( $p = 0.061$  based on ANOVA), due to the broad distribution of pKa values in each group. The differences in pKa values in the total oxidation group are almost negligible ( $p = 0.752$ ) (Fig. 3B). The surface accessibility of Cys residues is another important factor associated with the redox sensitivity of protein thiols. As expected, Cys residues with higher SSG occupancies had a significantly larger surface accessibility (Fig. 3A). For example, ~45% of Cys sites in SSG-5 subgroup were identified as solvent-exposed sites (with a RSA > 25%). This percentage was much higher than the values in other low SSG subgroups (i.e. < 39%). A similar, but less obvious, trend was observed for total oxidation, suggesting that surface accessibility is likely more important for SSG formation.

Analysis of the secondary structure of Cys residues showed that highly oxidized thiols had higher propensity to localize in structurally

flexible regions. For instance, ~60% of Cys residues in SSG5 and Oxi5 subgroups were localized to loop and coil structures (Fig. S2). Statistical analyses also showed that the higher occupancy groups were significantly more likely to localize in loop and coil structures (Fig. S2B). These flexible structures are usually beneficial for the formation of protein disulfides and other redox modifications due to less structural constraints [54]. Analysis of flanking sequence of Cys residues also revealed that the more oxidized thiols were characterized with substantially higher hydrophilicity (negative GRAVY score) and significantly lower stability (low Aliphatic index) compared to the more reduced thiols (Fig. 3). The formation of Cys modifications such as SSG and disulfide might serve as a key regulator to stabilize protein structures and to modulate protein surface properties under physiological conditions [54]. By contrast, more reduced Cys sites were predominantly located in  $\alpha$ -helices or  $\beta$ -sheets (~60%) that are usually buried within ordered protein structures (Fig. S2).

In addition, we found that no specific primary sequence motifs exist in Cys-containing peptides, which was consistent with previous studies [55–57]. However, over-representation of a second Cys residue in the –2 or +2 position of oxidized Cys sites was observed for protein cysteines in the SSG5 group (Fig. S3), suggesting a CXC motif is favorable for Cys residues with high levels of SSG modification. The CXC motif is also associated with active Cys sites that had similar activity as disulfide isomerase, but its biological function is still unknown [58,59].

### 3.3. Subcellular redox compartmentalization based on occupancy data

Cellular redox compartmentalization has been previously reported with different organelles displaying different redox potentials [60]. Herein we examine whether the levels of redox PTM occupancies on protein Cys residues will reveal such subcellular compartmentalization in macrophages. The identified proteins were distributed across all major cellular compartments with a large proportion in the cytoplasm (37.1%), nucleus (32.3%), and mitochondria (8.7%) (Fig. S4, Table S2). The subcellular distribution pattern was comparable to that of the whole proteome of *Mus musculus*, suggesting no significant bias exists in our redox proteomics workflow. Therefore, this large redox proteomics dataset with relatively broad proteome coverage enabled us to assess the redox status of protein thiols in different organelles.

Fig. 4A shows the average occupancy for SSG and total oxidation in major cellular organelles or compartments. As expected, distinct subcellular compartments also displayed significant differences in terms of distribution of site occupancies for both PTMs (Fig. S5), reflecting substantial differences in thiol-disulfide equilibrium in individual compartments. To accomplish specific cellular functions, organelles must maintain distinct redox status [60,61], which can be quantified based on the steady-state redox potentials of GSH/GSSG ratio or Trx enzymes [62]. A good correlation between the mean site occupancies of both SSG and total oxidation for individual compartments and the estimated subcellular redox potentials was also observed. For example, the mean SSG occupancy in reducing compartments such as the mitochondria (non-membrane) and nucleus (3.39% and 3.81%, respectively) were significantly lower than those in other more oxidizing organelles (e.g., lysosome, and ER). The reported redox potentials of Trx enzymes in mitochondria and nuclei are –360 mV and –300 mV respectively, which are substantially lower than the value (i.e., –240 to –220 mV) measured for the entire cell [62,63]. Higher levels of occupancies for both SSG and total oxidation were also observed for the mitochondrial membrane component compared to those in the non-membrane portion of mitochondria. This is consistent with the knowledge that the mitochondria maintain a more oxidizing environment in the membrane rather than in the matrix for ROS generation [64]. Furthermore, the mean occupancy for both SSG and total oxidation were much higher in the endoplasmic reticulum (ER, 4.49% and 17.4%, respectively) and lysosome (4.25% and 14.3%, respectively), two of the most oxidizing organelles [63,65], than other subcellular compartments. The

**Table 1**  
**Site occupancies of redox PTMs for selected proteins in different functional categories.**

Protein ID	Protein Description	Subcellular Localization <sup>a</sup>	Cys-sites <sup>b</sup>	Site occupancies		
				SSG (%)	T_oxi (%)	Log <sub>2</sub> FC
<b>Thioredoxin &amp; Glutaredoxin Systems</b>						
THIO	Thioredoxin	N; C; S	32 <sup>#</sup> &35 <sup>#</sup> 46 73 <sup>@</sup>	1.5 0.8 1.0	9.2 2.5	0.3 0.2 0.3
THIOM	Mitochondrial thioredoxin	M	90 <sup>#</sup> &93 <sup>#</sup>		15.8	
TRXR2	Thioredoxin reductase 2, mito	M	86 <sup>S</sup> &9 <sup>S</sup>	2.2	12.9	
TXND5	Thioredoxin domain-containing (DC) protein 5	ER	107&114 203 <sup>S</sup> &206 <sup>S</sup> 233&240 335 <sup>S</sup> &338 <sup>S</sup>	4.8	82.2 10.1 23.5 11.2	0 0.8  -0.3
TXD12	Thioredoxin DC 12 (Erp19)	ER	64 <sup>S</sup> &67 <sup>S</sup>	5.1	13.3	
TXD17	Thioredoxin DC 17	C	43 <sup>#</sup> &46 <sup>#</sup>	3	16.6	
GLRX2	Glutaredoxin-2, mitochondrial	M; N M; N	70 <sup>S</sup> &73 <sup>S</sup> 146 <sup>§</sup>	8.5 3.1	17.5 15.4	
PRDX1	Peroxiredoxin-1	C	52 <sup>#</sup>		11.8	0.5
PRDX2	Peroxiredoxin-2	C	70		11.8	
PRDX4	Peroxiredoxin-4	C; ER	54	21.1	34.6	0.2
PRDX5	Peroxiredoxin-5	M; P	96 <sup>#</sup>	2.4	10.2	0.3
PRDX6	Peroxiredoxin-6	C; L	47 <sup>#</sup>	14.7	50.2	0.1
<b>Protein disulfide isomerases</b>						
PDIA1	Protein disulfide-isomerase	ER; ML	55 <sup>#</sup> ,58 <sup>#</sup> 314 345 399 <sup>S</sup>	4.6 2.1 2.8	13.2 4.2 26.8	1.3 0.8 0.9 1.2
PDIA3	Protein disulfide-isomerase A3	ER; ML	57 <sup>#</sup> 60 <sup>#</sup> 85 <sup>S</sup> ,92 <sup>S</sup> 244		19.9 14.4 73.9 8.8	1.1 1.1 0.1 0.7
PDIA4	Protein disulfide-isomerase A4	ER; ML	548 <sup>S</sup> ,551 <sup>S</sup>		10.6	0.6
PDIA6	Protein disulfide-isomerase A6	ER; ML	291,297		24.0	0.3
<b>Ion channels, transporters and other membrane proteins</b>						
AT2A2	Sarcoplasmic/ER calcium ATPase 2	ER	364 498	26.0 8.2	29.3 6.6	0.5 0.4
SO4A1	Solute carrier organic anion transporter family member 4A1	CM	506 <sup>S</sup> ,511 <sup>S</sup> ,512 <sup>S</sup>	40.1	76.5	0.6
AT1B3	K-transporting ATPase subunit beta-3	CM; ML	144 <sup>S</sup> &154 <sup>S</sup> 191 <sup>S</sup> 249 <sup>S</sup>	0.6 1.1 6.7	22.0 37.4 40.9	0.5 0.4 0.3
CD68	Macrosialin	EM; LM	22 283&286 <sup>S</sup>	22.7 3.5	33.7 47.3	0.4 0.3
ICAM1	Intercellular adhesion molecule 1	CM	134 239 <sup>S</sup> 292 334 422 <sup>S</sup>	8.7 2.4   3.6	24.4 21.1 33.6 87.1 51.5	 -0.1   0.3
ITB2	Integrin beta-2	CM	287 <sup>S</sup> 387 550 <sup>S</sup> 583 <sup>S</sup> 672	5.2 29.2 7.4 9.2 6.8	30.8 47.2 101.2 81.2 25.9	0.5 0.4 0.4 0.5 0.3
MPRI	Cation-independent mannose-6-phosphate receptor	LM	129 <sup>S</sup> 169 <sup>S</sup> 223 <sup>S</sup> &230 <sup>S</sup> 724 <sup>S</sup> 823 1035 1220 1275 1469	3.3 10.6 8.3 14.8 24.1 14.8 35.3 24.5 8.1	53.2 61.1 60.1 61.7 64.6 45.7 97.1 76.0 62.9	0.2 0.2 0.1 0.3 0.1 0.2 0.0 0.1 0.3
LRP1	Prolow-density lipoprotein receptor-related protein 1	CM; N; C	808 <sup>S</sup> 3295 <sup>S</sup> 3474	9.0 6.9 25.4	49.2 23.6 64.2	0.4 0.3 0.4
<b>Other proteins</b>						
MT1	Metallothionein-1	C; L; N	44,48,50	33.3	16.9	0.8
MT2	Metallothionein-2	C; N	33,36,41	16.9	14.6	0.8
CATB	Cathepsin B	L; ML; EX	93 105 211	10.5 2.7 17.5	45.0 22.4 71.3	0.3 0.3 0.3
ENV1	MLV-related proviral Env polyprotein	CM	131 162 181 356 <sup>S</sup>		66.1 83.8 72.0 63.5	0.3 0.4 0.4 0.1
GANAB	Neutral alpha-glucosidase AB	ER; G; ML	41 <sup>S</sup> & 47 <sup>S</sup>	2.6	90.5	0.7

(continued on next page)

Table 1 (continued)

Protein ID	Protein Description	Subcellular Localization <sup>a</sup>	Cys-sites <sup>b</sup>	Site occupancies		
				SSG (%)	T <sub>oxi</sub> (%)	Log <sub>2</sub> FC
HEXB	Beta-hexosaminidase subunit beta	L	633&644	6.6	21.5	0.7
			288 <sup>S</sup>		62.9	
			530 <sup>S</sup>		50.7	
ICA	Inhibitor of carbonic anhydrase	S	185&188	8.7	50.8	0.4

<sup>a</sup> Notation for subcellular localization: C = Cytoplasm; CM = cell membrane; CS = cytoskeleton; EM = endosome membrane; ER = endoplasmic/sarcoplasmic reticulum; EX = extracellular; G = Golgi apparatus; L = lysosome; LM = lysosome membrane; M = mitochondria; ML = melanosome; N = nucleus; P = peroxisome; S = secreted.

<sup>b</sup> # = active sites; @ = Previously reported sites of S-glutathionylation; § = binding sites (such as to metal) S = disulfide.

correlation between the occupancies of thiol redox modifications and the redox potentials of organelles further support a potential critical role of protein thiols in maintaining subcellular redox states and redox signaling.

Fig. 4B further illustrates a subcellular landscape of protein redox networks for selected proteins displaying different levels of total oxidation in terms of site occupancies. Specific proteins from different functional classes along with their site occupancy data are listed in Table 1. Proteins with high occupancies were observed to be localized to the plasma membrane and ER.

### 3.4. Subcellular susceptibility to oxidative stress perturbations

The relative changes of site occupancy in response to oxidative stress may provide insights into their biological functions. Recently, we reported a detailed analysis of the changes in protein-SSG modifications in macrophages following oxidative stress perturbation induced by exposure to several metal oxide ENPs [21]. It is well-documented that various metal oxide ENPs are able to generate ROS either directly by their surface chemistries or indirectly by modulating endogenous sources of ROS production [66]. More importantly, ROS generation and signaling through protein-SSG are likely the key initiating events in modulating various biological responses in macrophages [21,22,67]. Since the basal-level SSG occupancy has been defined in this work, we further assessed the shift of SSG occupancy following ENP exposure for 879 Cys sites from 557 proteins based on the previously reported data on relative changes in SSG (Supporting Data 1). These proteins covered over 65% of all identified proteins in our previous experiment. Both Fe<sub>3</sub>O<sub>4</sub> and CoO ENPs induced ROS with significant changes in SSG levels in macrophages (p-value < 0.001), with a more substantial change observed under CoO treatment. This was in line with the fact that Fe<sub>3</sub>O<sub>4</sub> and CoO lead to low and high levels of cellular oxidative stress, respectively [21].

While the details of Cys sites sensitive to oxidative stress have been previously described [21], we assessed the subcellular susceptibility in terms of changes in SSG occupancy following exposure to ENPs (Fig. 5). For Fe<sub>3</sub>O<sub>4</sub>, the average SSG occupancy increased by 4–6% (p-value < 0.001) in reducing compartments such as the nucleus, cytoskeleton and mitochondria (non-membrane), while no significant changes were observed in oxidizing organelles such as the ER and Golgi apparatus. The lack of significant changes of SSG in oxidizing organelles under low level of oxidative stress is not surprising since most protein thiols involved in protein folding are highly oxidized under basal conditions and it may take much higher level of oxidative stress to alter the redox state of these proteins.

By contrast, CoO had a much broader impact, leading to a much higher percentage increase of SSG in all major compartments compared to Fe<sub>3</sub>O<sub>4</sub> treatment. Peroxisome, ER, and mitochondria (membrane) were most affected with an average of 15–27% increase in SSG occupancy. Interestingly, these three components are the well-known cellular compartments for ROS production under oxidative stress [68]. By contrast, protein thiols in the mitochondrial (non-membrane) matrix and the Golgi apparatus were the most resistant to CoO-induced oxidative stress, which might be attributed to the unique antioxidant

systems in Golgi [69] or the high antioxidant capacity of mitochondria [70]. It is interesting to observe that mitochondria (non-membrane) is one of the two components most resistant to oxidative stress perturbation. While mitochondria are generally considered one of the main sources of endogenous ROS, they also have unique antioxidant capacity including high concentrations of antioxidant defense enzymes to serve as a cellular H<sub>2</sub>O<sub>2</sub> stabilizing device [70]. Therefore, the observation of the resistance to oxidative stress in mitochondria (non-membrane) is consistent with the knowledge that the mitochondrial matrix is the most reducing of cellular compartments (Fig. 4A) with high antioxidant capacity. It is likely that most of the oxidative susceptibility lies in the membrane component of mitochondria. Finally, it appears that protein thiols located in the nuclei, cytoplasm, and cytoskeleton are sensitive to even low levels of oxidative stress.

### 3.5. Other functional implications from the occupancy data of redox PTMs

The thiol redox proteome covered a broad range of functional categories including the thioredoxin/glutaredoxin systems, protein disulfide isomerases, ion channels, transporters and other membrane proteins, as well as various other enzymes. Table 1 lists selected proteins from different classes along with their subcellular location and site occupancy data. Proteins involved in the thioredoxin/glutaredoxin system generally had lower levels of occupancy (10–20%) in SSG and total oxidation under basal conditions, consistent with the knowledge that these enzymes are active in a reduced state and must remain active due to their critical roles as in the reduction of protein thiols. By contrast, some protein disulfide-isomerases, key enzymes facilitating protein folding in the endoplasmic reticulum (ER), and enzymes localized in lysosomes such as Cathepsins had much higher occupancies in terms of total oxidation (>50%) and many of these highly oxidized Cys sites are known to form disulfides. Ion channels, transporters, and other membrane proteins were also often observed to have high occupancy of total oxidation, supporting that protein disulfides in transmembrane proteins are often required for their stability and function [71].

To further explore the functional implications of the basal site occupancies, we compared the occupancy distribution of active cysteine sites to that of non-active Cys sites from the same set of proteins. Higher occupancies were observed for both SSG and total oxidation and the SSG occupancy was significantly higher in the active site group (Fig. S6). The difference in total oxidation between active sites and non-active sites was not significant, presumably due to some high occupancy non-active Cys sites serving as structural disulfides. We further examined whether active Cys sites generally have higher occupancies by comparing non-active site Cys residues from the same protein. Fifteen proteins were compiled with occupancies for both non-active and active Cys sites (Fig. S7), and 11 of them (DUS3, G3P, G3PT, GMPR1, PCKGM, PDIA1, PTN6, SAE2, THIO, UBA1Y, and UBC12) displayed higher site occupancies in the active Cys sites (representative ones shown in Fig. 6). Non-active Cys sites displaying higher occupancies are often part of known disulfides (e.g., CATB, PDIA3). Guanosine monophosphate reductase 1 (GMPR1) is an interesting example in which the enzyme

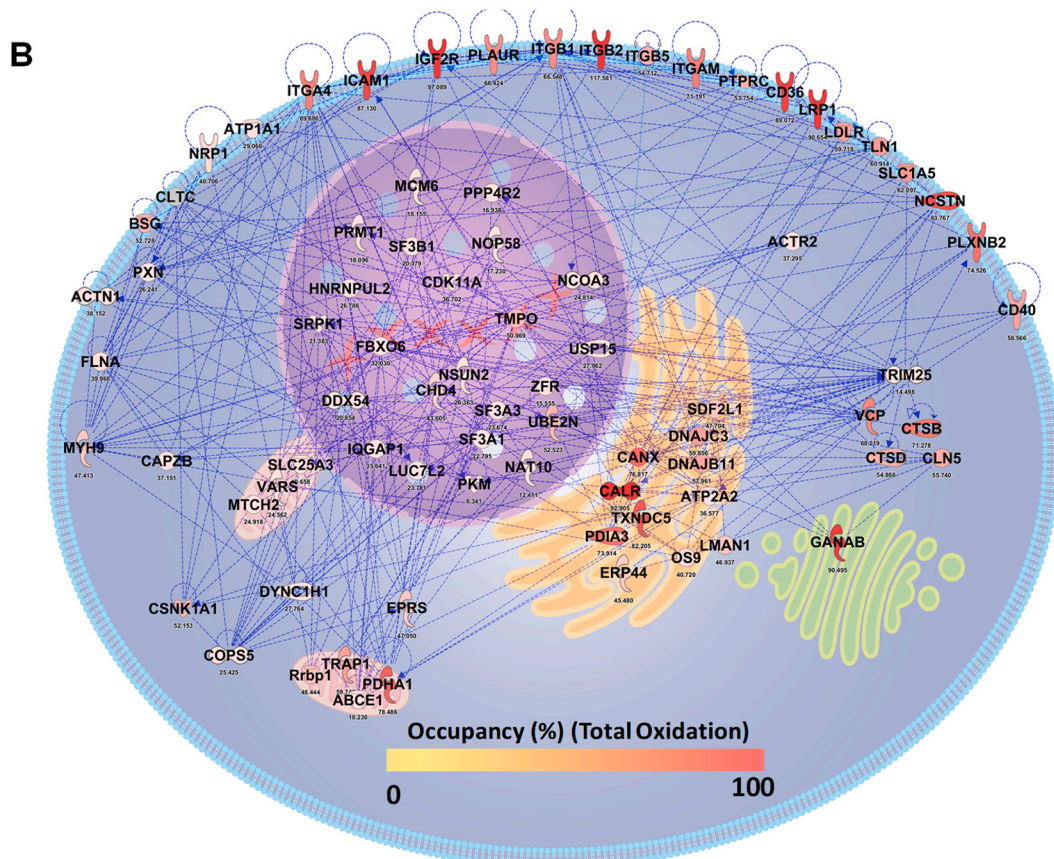
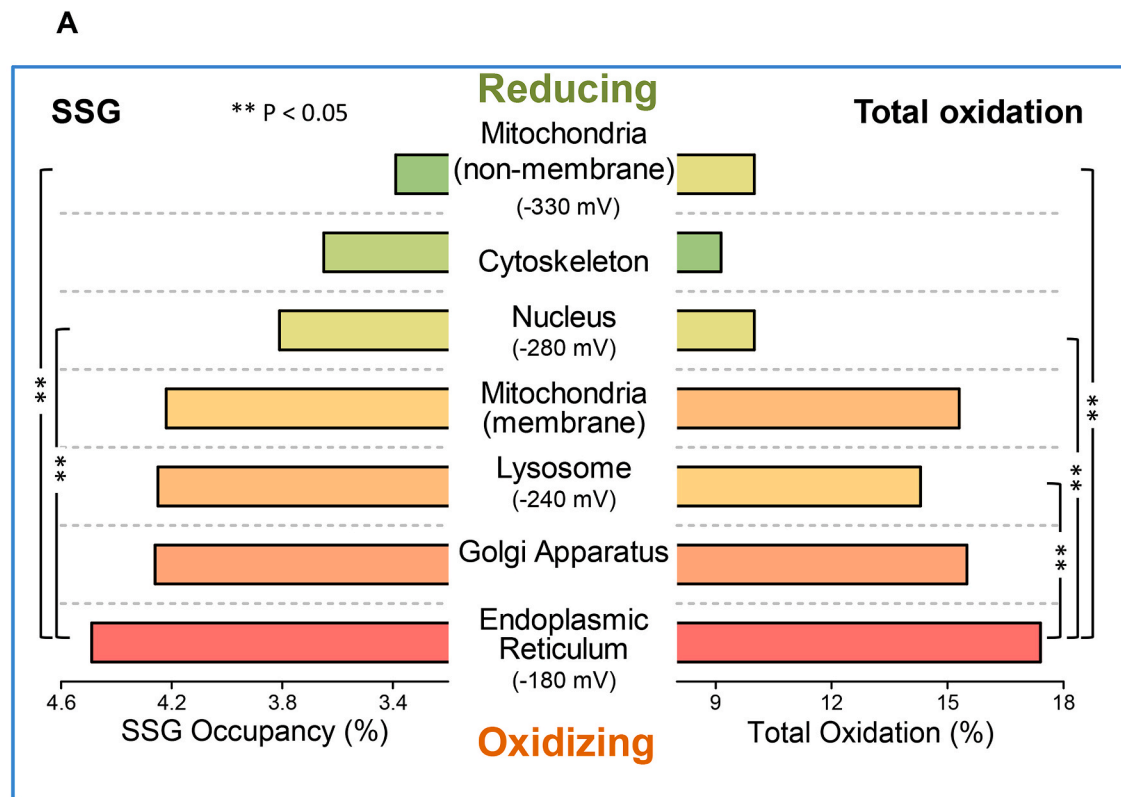


**Fig. 4.** The average occupancies of redox PTMs are correlated with the redox potential of subcellular compartments. (A) Major organelles were ranked by their redox potentials, and the average occupancy of SSG (left) and total oxidation (right) of proteins in these organelles were plotted. Note that mitochondrial membrane and non-membrane components were separately annotated. Subcellular localization annotation was based on the MetazSecKB Database <http://bioinformatics.ysu.edu/secretomes/animal/index.php> (B) A subcellular map of redox networks with protein thiol redox state based on total oxidation occupancy being highlighted.

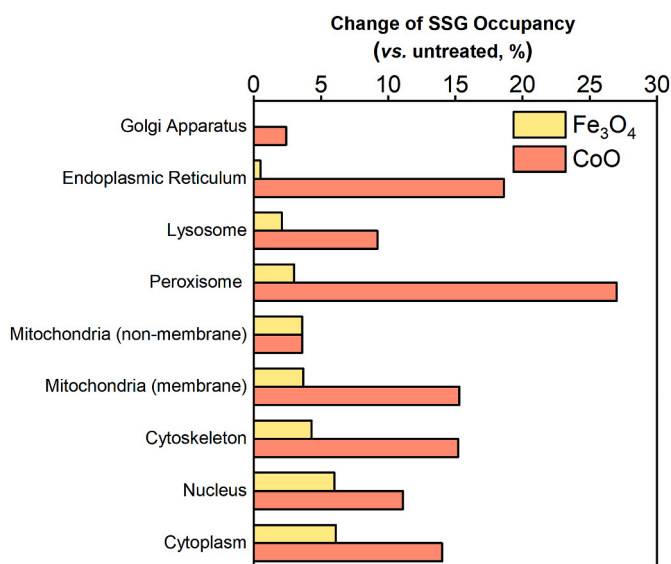


**Fig. 5.** Change of SSG occupancy under oxidative stress induced by nanoparticles. The percentage increase of SSG occupancy upon treatment in major cellular organelles was shown.

activity is likely regulated by the redox state of the active site Cys186. We observed that Cys186 of GMPR1 had an occupancy of ~50% SSG at basal levels, which is consistent with a previous biochemical report that the enzyme inactivation can be prevented or reversed by reducing sulfhydryl compounds [72]. Taken together, this data supports that

protein cysteines in the enzymatic active sites generally have higher levels of occupancy compared to those of non-active Cys residues.

Cys sites with varying degrees of occupancy may also play distinct functional roles in regulation of protein activity and pathways. We speculated that protein thiols with low- and high-SSG occupancy may activate and inhibit specific pathways, respectively, under oxidative stress. We tested this hypothesis with Cys sites with statistically significant changes following CoO exposure (Fig. S8). Following the treatment, low-occupancy sites were enriched in processes such as glycolysis, metabolic pathways, and protein processing in ER, which could be activated for adaptive responses (Fig. S8A). Activation of these pathways may be associated with metabolic reconfiguration and altered protein turnover in response to oxidative stress [73–75]. By contrast, pathways such as FcR-mediated phagocytosis were inhibited under oxidative stress (Fig. S8B), as demonstrated by the phagocytic activity of macrophage being highly suppressed after CoO treatment [21]. Other suppressed pathways include aminoacyl-tRNA biosynthesis and protein processing in ER, which correspond to inhibition of protein translation and ER function during oxidation stress [21,76].

#### 4. Discussion

Macrophages play a critical role in regulating the innate immune response and inflammation [77]. Dysfunction of macrophages is associated with pathogenesis and progression of many diseases including autoimmune disorders and cancers [78,79], in which ROS-mediated redox signaling plays an essential role [80]. Reversible redox modifications of proteins are considered key events in these processes. Information on the site occupancy of specific PTMs would enable a better understanding of their biological functions. Herein, we simultaneously

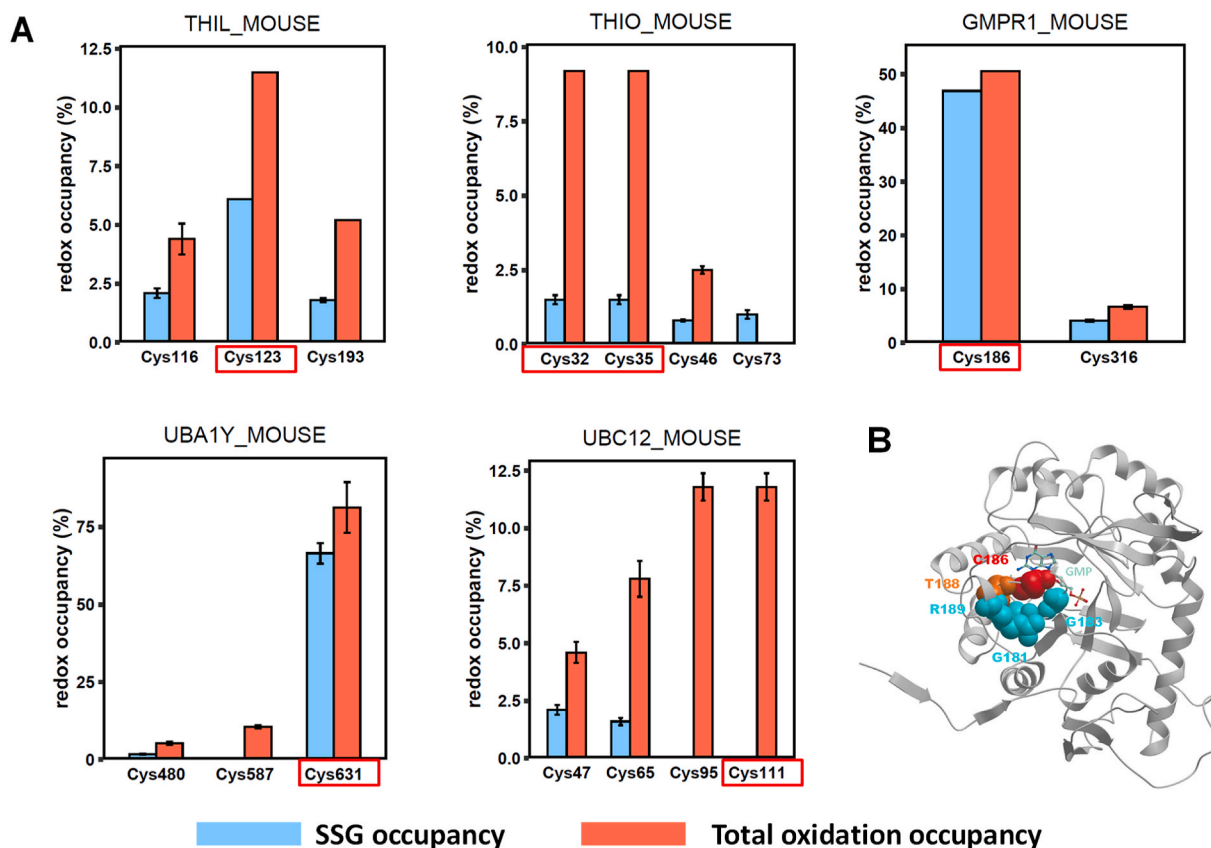


**Fig. 6.** Cysteine residues serving as active sites tend to have higher occupancies comparing to other cysteine residues on the same protein. (A) Representative proteins with cysteine residues as the active site. For each protein, the SSG occupancy (blue bar) and total oxidation occupancy (orange bar) for each cysteine site were plotted. Error bars represent standard deviations across four replicates. Active sites were highlighted in red boxes. (B) Structure of GMPR1 with the active site Cys186 highlighted. (For interpretation of the references to colour in this figure legend, the reader is referred to the Web version of this article.)

measured the site occupancy of SSG and total reversible thiol oxidation for ~4099 Cys sites in mouse macrophages. Recently, a number of proteomics methods have been reported for profiling SSG, including the utilization of clickable probes [81,82] and mercury resin-based enrichment coupled with selective reduction [57]. Our recent reports on SSG in mouse muscle and macrophages [21,31,83] along with the current data demonstrates that the RAC-TMT method not only provides improved quantitative measurements of site occupancy, but also much deeper coverage of the thiol proteome. The stoichiometric measurements confirmed that protein-SSG modifications are highly heterogeneous, global cellular events. We also found that ~12% of protein thiols are reversibly oxidized and ~4% are subjected to SSG modification. The overall reduced status of protein thiols is in good agreement with the fact that cells maintain a highly reducing environment for normal physiological activities. In addition, the high ratio of SSG to total oxidation underscores SSG as a primary redox PTM of the cell.

Distinct subcellular compartments are critical for maintaining unique redox micro-environments in the cell for carrying out specific biological processes and redox signaling. Significant advances utilizing redox probes, such as genetic encoded proteins have been reported for imaging of defined redox species with subcellular resolution in living cells [84]. However, direct measurements of subcellular redox status at the proteome level remains challenging [60,61]. In this work we demonstrated that our redox proteomics approach provides an indirect characterization of the cellular and subcellular redox status by measuring SSG and total oxidation levels of protein thiols. Our results showed the redox status of subcellular components correlates well with the subcellular levels of SSG and Cys oxidation, by which reducing and oxidizing organelles can be easily distinguished. Proteins localized to mitochondria (non-membrane), nucleus, and cytoskeleton had relatively low levels of SSG and total oxidation, whereas protein in ER, Golgi apparatus, and lysosome tended to have higher levels of oxidation occupancy. Moreover, our results showed that cellular compartments displayed distinct patterns of susceptibility to changes in SSG in response to different levels of oxidative stress in macrophages exposed to ENPs [21]. For example, under moderate oxidative stress induced by Fe<sub>3</sub>O<sub>4</sub>, protein thiols in the nucleus, cytoskeleton and mitochondria (membrane) were more susceptible to SSG modification. By contrast, under higher levels of oxidative stress induced by CoO, peroxisome, ER and mitochondria (membrane), which are the three major sources of cellular ROS production [68], showed the most significant SSG increases compared to other compartments, supporting their critical roles in intracellular ROS signaling. This is in agreement with recent studies focused on the role of protein-SSG in mitochondrial function and in providing a negative feedback for regulating ROS production in mitochondria [81,85–87]. On the other hand, mitochondria (non-membrane) and Golgi apparatus appeared to be much less susceptible to redox changes under oxidative stress, suggesting a potential mechanism for compartment-specific redox regulation [69]. We note that several recent studies using different tissues (e.g., muscle, liver) [31,88] suggest mitochondria as focal points for SSG-mediated redox regulation. It is likely that mitochondrial redox changes are more localized to the membrane component rather than the non-membrane component. Together, our results shed valuable insights into subcellular redox regulation, which still requires more detailed investigation for a better mechanistic understanding.

The site occupancy data for individual proteins displayed in Table 1 provides information on protein function as well as functional sites. Indeed, a large number of Cys residues identified here were localized to annotated functional regions or domains and may potentially play regulatory roles. Reversible redox modifications at these functional sites may represent a sensitive mechanism to regulate protein functions and interactions by modulating protein structure in a redox-dependent manner. Function analysis showed that only ~4% of redox-modified Cys residues had been annotated as functional sites including active sites, metal-binding sites, nucleotide-binding sites and DNA-binding

sites. In general, we observed that protein active sites have a higher level of site occupancy compared to non-active sites of the same protein (Fig. 6, and Fig. S7). Thus, site occupancy data may serve as a predictor of protein functional sites. Finally, the regulatory roles of redox modifications could be achieved either by activating or inhibiting specific enzymes or biological pathways. The site occupancy data may also serve as an important resource to identify functional sites that serve activating or inhibiting functions. Taken together, our study provides a rich database for understanding redox signaling and regulation in macrophages while the basal occupancy data will provide a valuable baseline reference for future studies of macrophages as a model system with different stimuli such as cytokines.

## 5. Conclusions

The thiol redox proteome of macrophages under normal physiological conditions was profiled for the site occupancies of both SSG and total oxidation, providing several key findings and insights in redox-based regulation. First, subcellular compartmentalization of the redox landscape was verified at the proteome level based on the observation that the mean site occupancies of both SSG and total oxidation among distinct organelles correlate with their reported redox potentials. Moreover, a general association between structural features and site occupancy was also observed at the proteome level. Significantly, different degrees of occupancy of redox modifications are required for proteins to fulfill specific functions. Our data supported this notion by showing that the thioredoxin/glutaredoxin system maintains a low occupancy of redox modifications while enzymes involving in protein folding typically display a much higher degree of occupancy. Additionally, protein thiols on enzymatic active sites generally had higher levels of occupancy compared to non-active sites. Finally, the proteomics analyses not only provide an overview of the thiol redox landscape of macrophages under normal physiological conditions, but also can be used to assess the degree of susceptibility to redox changes under oxidative stress. Such analyses have the potential to reveal novel thiol-based mediators of redox signaling.

## Author disclosure statement

The authors declare no competing financial interests.

## Declaration of competing interest

The authors declare no conflict of interests.

## Acknowledgements

Portions of this work were supported by NIH grants R01 GM125968, R01 DK122160, and U01 ES027292. The experimental work described herein was performed in the Environmental Molecular Sciences Laboratory, Pacific Northwest National Laboratory, a national scientific user facility sponsored by the Department of Energy under Contract DE-AC05-76RL0 1830.

## Appendix A. Supplementary data

Supplementary data to this article can be found online at <https://doi.org/10.1016/j.redox.2020.101649>.

## References

- [1] F. Ursini, M. Maiorino, H.J. Forman, Redox homeostasis: the Golden Mean of healthy living, *Redox Biol.* 8 (2016) 205–215.
- [2] J. Duan, M.J. Gaffrey, W.J. Qian, Quantitative proteomic characterization of redox-dependent post-translational modifications on protein cysteines, *Mol. Biosyst.* 13 (5) (2017) 816–829.

- [3] J. Yang, K.S. Carroll, D.C. Liebler, The expanding landscape of the thiol redox proteome, *Mol. Cell. Proteomics* 15 (1) (2016) 1–11.
- [4] Y.M.W. Janssen-Heininger, B.T. Mossman, N.H. Heintz, H.J. Forman, B. Kalyanaraman, T. Finkel, J.S. Stamler, S.G. Rhee, A. van der Vliet, Redox-based regulation of signal transduction: principles, pitfalls, and promises, *Free Radic. Biol. Med.* 45 (1) (2008) 1–17.
- [5] C.E. Paulsen, K.S. Carroll, Cysteine-mediated redox signaling: chemistry, biology, and tools for discovery, *Chem. Rev.* 113 (7) (2013) 4633–4679.
- [6] C.C. Benz, C. Yau, Ageing, oxidative stress and cancer: paradigms in parallax, *Nat. Rev. Canc.* 8 (11) (2008) 875–879.
- [7] E. Mariani, M.C. Polidori, A. Cherubini, P. Mecocci, Oxidative stress in brain aging, neurodegenerative and vascular diseases: an overview, *J. Chromatogr. B* 827 (1) (2005) 65–75.
- [8] J.L. Rains, S.K. Jain, Oxidative stress, insulin signaling, and diabetes, *Free Radic. Biol. Med.* 50 (5) (2011) 567–575.
- [9] S. Reuter, S.C. Gupta, M.M. Chaturvedi, B.B. Aggarwal, Oxidative stress, inflammation, and cancer How are they linked? *Free Radic. Biol. Med.* 49 (11) (2010) 1603–1616.
- [10] M. Valko, D. Leibfritz, J. Moncol, M.T.D. Cronin, M. Mazur, J. Telser, Free radicals and antioxidants in normal physiological functions and human disease, *Int. J. Biochem. Cell Biol.* 39 (1) (2007) 44–84.
- [11] J.D. Short, K. Downs, S. Tavakoli, R. Asmis, Protein thiol redox signaling in monocytes and macrophages, *Antioxidants Redox Signal.* 25 (15) (2016) 816–835.
- [12] S. Ullevig, H.S. Kim, R. Asmis, S-glutathionylation in monocyte and macrophage (dys) function, *Int. J. Mol. Sci.* 14 (8) (2013) 15212–15232.
- [13] J.J. Mieyal, M.M. Gallogly, S. Qanungo, E.A. Sabens, M.D. Shelton, Molecular mechanisms and clinical implications of reversible protein S-glutathionylation, *Antioxidants Redox Signal.* 10 (11) (2008) 1941–1988.
- [14] A. Bachi, I. Dalle-Donne, A. Scaloni, Redox proteomics: chemical principles, methodological approaches and biological/biomedical promises, *Chem. Rev.* 113 (1) (2013) 596–698.
- [15] L.M. Lopez-Sanchez, C. Lopez-Pedraza, A. Rodriguez-Ariza, Proteomic approaches to evaluate protein S-nitrosylation in disease, *Mass Spectrom. Rev.* 33 (1) (2014) 7–20.
- [16] P.A. Kramer, J. Duan, W.J. Qian, D.J. Marcinek, The measurement of reversible redox dependent post-translational modifications and their regulation of mitochondrial and skeletal muscle function, *Front. Physiol.* 6 (2015) 347.
- [17] J.M. Held, B.W. Gibson, Regulatory control or oxidative damage? Proteomic approaches to interrogate the role of cysteine oxidation status in biological processes, *Mol. Cell. Proteomics* 11 (4) (2012).
- [18] Y.J. Chen, C.T. Lu, T.Y. Lee, Y.J. Chen, dBSH: a database of S-glutathionylation, *Bioinformatics* 30 (16) (2014) 2386–2388.
- [19] Y.-J. Chen, C.-T. Lu, M.-G. Su, K.-Y. Huang, W.-C. Ching, H.-H. Yang, Y.-C. Liao, Y.-J. Chen, T.-Y. Lee, dbSNO 2.0: a resource for exploring structural environment, functional and disease association and regulatory network of protein S-nitrosylation, *Nucleic Acids Res.* 43 (D1) (2015) D503–D511.
- [20] M.A. Sun, Y.J. Wang, H. Cheng, Q. Zhang, W. Ge, D.J. Guo, RedoxDB—a curated database for experimentally verified protein oxidative modification, *Bioinformatics* 28 (19) (2012) 2551–2552.
- [21] J. Duan, V.K. Kodali, M.J. Gaffrey, J. Guo, R.K. Chu, D.G. Camp, R.D. Smith, B. D. Thrall, W.J. Qian, Quantitative profiling of protein S-glutathionylation reveals redox-dependent regulation of macrophage function during nanoparticle-induced oxidative stress, *ACS Nano* 10 (1) (2016) 524–538.
- [22] T. Zhang, M.J. Gaffrey, W.-J. Qian, B.D. Thrall, Oxidative stress and redox modifications in nanomaterial–cellular interactions, in: J.C. Bonner, J.M. Brown (Eds.), *Interaction of Nanomaterials with the Immune System*, Springer International Publishing, Cham, 2020, pp. 127–148.
- [23] K. Wojdyła, A. Rogowska-Wrzesinska, Differential alkylation-based redox proteomics - lessons learnt, *Redox Biol.* 6 (2015) 240–252.
- [24] C.I. Murray, J.E. Van Eyk, A twist on quantification measuring the site occupancy of S-nitrosylation, *Circ. Res.* 111 (10) (2012) 1253–1255.
- [25] J. Guo, A.Y. Nguyen, Z. Dai, D. Su, M.J. Gaffrey, R.J. Moore, J.M. Jacobs, M. E. Monroe, R.D. Smith, D.W. Koppenaal, H.B. Pakrasi, W.J. Qian, Proteome-wide light/dark modulation of thiol oxidation in cyanobacteria revealed by quantitative site-specific redox proteomics, *Mol. Cell. Proteomics* 13 (12) (2014) 3270–3285.
- [26] N. Brandes, D. Reichmann, H. Tienson, L.I. Leichere, U. Jakob, Using quantitative redox proteomics to dissect the yeast redoxome, *J. Biol. Chem.* 286 (48) (2011) 41893–41903.
- [27] N. Brandes, H. Tienson, A. Lindemann, V. Vitvitsky, D. Reichmann, R. Banerjee, U. Jakob, Time line of redox events in aging postmitotic cells, *Elife* 2 (2013).
- [28] D. Knoefler, M. Thamsen, M. Koniczek, N.J. Niemuth, A.-K. Diederich, U. Jakob, Quantitative in vivo redox sensors uncover oxidative stress as an early event in life, *Mol. Cell* 47 (5) (2012) 767–776.
- [29] K.E. Menger, A.M. James, H.M. Cocheme, M.E. Harbour, E.T. Chouchani, S. Ding, I. M. Fearnley, L. Partridge, M.P. Murphy, Fasting, but not aging, dramatically alters the redox status of cysteine residues on proteins in *Drosophila melanogaster*, *Cell Rep.* 11 (12) (2015) 1856–1865.
- [30] S. Rosenwasser, S.G. van Creveld, D. Schatz, S. Malitsky, O. Tzfadia, A. Aharoni, Y. Levin, A. Gabashvili, E. Feldmesser, A. Vardi, Mapping the diatom redox-sensitive proteome provides insight into response to nitrogen stress in the marine environment, *Proc. Natl. Acad. Sci. U.S.A.* 111 (7) (2014) 2740–2745.
- [31] P.A. Kramer, J. Duan, M.J. Gaffrey, A.K. Shukla, L. Wang, T.K. Bammler, W.J. Qian, D.J. Marcinek, Fatiguing contractions increase protein S-glutathionylation occupancy in mouse skeletal muscle, *Redox Biol.* 17 (2018) 367–376.
- [32] H. Xiao, M.P. Jedrychowski, D.K. Schweppe, E.L. Huttlin, Q. Yu, D.E. Heppner, J. Li, J. Long, E.L. Mills, J. Szpyt, Z. He, G. Du, R. Garrity, A. Reddy, L.P. Vaites, J. A. Paulo, T. Zhang, N.S. Gray, S.P. Gygi, E.T. Chouchani, A quantitative tissue-specific landscape of protein redox regulation during aging, *Cell* 180 (5) (2020) 968–983 e24.
- [33] J.B. Behring, S. van der Post, A.D. Mooradian, M.J. Egan, M.I. Zimmerman, J. L. Clements, G.R. Bowman, J.M. Held, Spatial and temporal alterations in protein structure by EGF regulate cryptic cysteine oxidation, *Sci. Signal.* 13 (615) (2020).
- [34] J. Guo, M.J. Gaffrey, D. Su, T. Liu, D.G. Camp, II, R.D. Smith, W.-J. Qian, Resin-assisted enrichment of thiols as a general strategy for proteomic profiling of cysteine-based reversible modifications, *Nat. Protoc.* 9 (1) (2014) 64–75.
- [35] J. Guo, A.Y. Nguyen, Z. Dai, D. Su, M.J. Gaffrey, R.J. Moore, J.M. Jacobs, M. E. Monroe, R.D. Smith, D.W. Koppenaal, H.B. Pakrasi, W.-J. Qian, Proteome-wide light/dark modulation of thiol oxidation in cyanobacteria revealed by quantitative site-specific redox proteomics, *Mol. Cell. Proteomics* 13 (12) (2014) 3270–3285.
- [36] D. Su, M.J. Gaffrey, J. Guo, K.E. Hatchell, R.K. Chu, T.R. Claus, J.T. Aldrich, S. Wu, S. Purvine, D.G. Camp, R.D. Smith, B.D. Thrall, W.J. Qian, Proteomic identification and quantification of S-glutathionylation in mouse macrophages using resin-assisted enrichment and isobaric labeling, *Free Radic. Biol. Med.* 67 (2014) 460–470.
- [37] H.S. Kim, S.L. Ullevig, D. Zamora, C.F. Lee, R. Asmis, Redox regulation of MAPK phosphatase 1 controls monocyte migration and macrophage recruitment, *Proc. Natl. Acad. Sci. U. S. A.* 109 (41) (2012) E2803–E2812.
- [38] J. Sakai, J. Li, K.K. Subramanian, S. Mondal, B. Bajrami, H. Hattori, Y. Jia, B. C. Dickinson, J. Zhong, K. Ye, C.J. Chang, Y.S. Ho, J. Zhou, H.R. Luo, Reactive oxygen species-induced actin glutathionylation controls actin dynamics in neutrophils, *Immunity* 37 (6) (2012) 1037–1049.
- [39] S.L. Ullevig, H.S. Kim, J.D. Short, S. Tavakoli, S.T. Weintraub, K. Downs, R. Asmis, Protein S-glutathionylation mediates macrophage responses to metabolic cues from the extracellular environment, *Antioxidants Redox Signal.* 25 (15) (2016) 836–851.
- [40] J. Guo, A.Y. Nguyen, Z. Dai, D. Su, M.J. Gaffrey, R.J. Moore, J.M. Jacobs, M. E. Monroe, R.D. Smith, D.W. Koppenaal, H.B. Pakrasi, W.-J. Qian, Proteome-wide light/dark modulation of thiol oxidation in cyanobacteria revealed by quantitative site-specific redox proteomics, *Mol. Cell. Proteomics* 13 (12) (2014) 3270–3285.
- [41] S. Kim, P.A. Pevzner, MS-GF plus makes progress towards a universal database search tool for proteomics, *Nat. Commun.* 5 (2014).
- [42] L. Kall, J.D. Storey, M.J. MacCoss, W.S. Noble, Assigning significance to peptides identified by tandem mass spectrometry using decoy databases, *J. Proteome Res.* 7 (1) (2008) 29–34.
- [43] J.Q. Fan, P. Tam, G.V. Woude, Y. Ren, Normalization and analysis of cDNA microarrays using within-array replications applied to neuroblastoma cell response to a cytokine, *Proc. Natl. Acad. Sci. U.S.A.* 101 (5) (2004) 1135–1140.
- [44] D.W. Huang, B.T. Sherman, R.A. Lempicki, Systematic and integrative analysis of large gene lists using DAVID bioinformatics resources, *Nat. Protoc.* 4 (1) (2009) 44–57.
- [45] T.-Y. Lee, Y.-J. Chen, C.-T. Lu, W.-C. Ching, Y.-C. Teng, H.-D. Huang, Y.-J. Chen, dbSNO: a database of cysteine S-nitrosylation, *Bioinformatics* 28 (17) (2012) 2293–2295.
- [46] M.H.M. Olsson, C.R. Sondergaard, M. Rostkowski, J.H. Jensen, PROPKA3: consistent treatment of internal and surface residues in empirical pKa predictions, *J. Chem. Theor. Comput.* 7 (2) (2011) 525–537.
- [47] B. Petersen, T.N. Petersen, P. Andersen, M. Nielsen, C. Lundegaard, A generic method for assignment of reliability scores applied to solvent accessibility predictions, *BMC Struct. Biol.* 9 (2009).
- [48] J. Meinken, G. Walker, C. Cooper, X.J. Min, *MetazSecKB: the human and animal secretome and subcellular proteome knowledgebase*, Database 2015 (2015), bav007, <https://doi.org/10.1093/database/bav077>.
- [49] J. Paulech, K.A. Liddy, K. Engholm-Keller, M.Y. White, S.J. Cordwell, Global analysis of myocardial peptides containing cysteines with irreversible sulfinic and sulfonic acid post-translational modifications, *Mol. Cell. Proteomics* 14 (3) (2015) 609–620.
- [50] R.E. Hansen, D. Roth, J.R. Winther, Quantifying the global cellular thiol-disulfide status, *Proc. Natl. Acad. Sci. U.S.A.* 106 (2) (2009) 422–427.
- [51] J. Kyte, R.F. Doolittle, A simple method for displaying the hydropathic character of a protein, *J. Mol. Biol.* 157 (1) (1982) 105–132.
- [52] A. Ikai, Thermostability and aliphatic index of globular-proteins, *J. Biochem.* 88 (6) (1980) 1895–1898.
- [53] S.M. Marino, V.N. Gladyshev, Redox biology: computational approaches to the investigation of functional cysteine residues, *Antioxidants Redox Signal.* 15 (1) (2011) 135–146.
- [54] M.V. Trivedi, J.S. Laurence, T.J. Siahhan, The role of thiols and disulfides on protein stability, *Curr. Protein Pept. Sci.* 10 (6) (2009) 614–625.
- [55] E. Weerapana, C. Wang, G.M. Simon, F. Richter, S. Khare, M.B.D. Dillon, D. A. Bachovchin, K. Mowen, D. Baker, B.F. Cravatt, Quantitative reactivity profiling predicts functional cysteines in proteomes, *Nature* 468 (7325) (2010), 790–U79.
- [56] S.M. Marino, V.N. Gladyshev, Structural analysis of cysteine S-nitrosylation: a modified acid-based motif and the emerging role of trans-nitrosylation, *J. Mol. Biol.* 395 (4) (2010) 844–859.
- [57] N.S. Gould, P. Evans, P. Martinez-Acedo, S.M. Marino, V.N. Gladyshev, K. S. Carroll, H. Ischiropoulos, Site-specific proteomic mapping identifies selectively modified regulatory cysteine residues in functionally distinct protein networks, *Chem. Biol.* 22 (7) (2015) 965–975.
- [58] K.J. Woycechowsky, R.T. Raines, The CXC motif: a functional mimic of protein disulfide isomerase, *Biochemistry* 42 (18) (2003) 5387–5394.
- [59] U. Derewenda, T. Boczek, K.L. Gorres, M. Yu, L.W. Hung, D. Cooper, A. Joachimiak, R.T. Raines, Z.S. Derewenda, Structure and function of Bacillus

- subtilis YphP, a prokaryotic disulfide isomerase with a CXC catalytic motif, *Biochemistry* 48 (36) (2009) 8664–8671.
- [60] D.P. Jones, Y.M. Go, Redox compartmentalization and cellular stress, *Diabetes Obes. Metabol.* 12 (2010) 116–125.
- [61] Y.M. Go, D.P. Jones, Redox compartmentalization in eukaryotic cells, *Biochim. Biophys. Acta Gen. Subj.* 1780 (11) (2008) 1271–1290.
- [62] Y.M. Go, D.P. Jones, Redox control systems in the nucleus: mechanisms and functions, *Antioxidants Redox Signal.* 13 (4) (2010) 489–509.
- [63] C. Hwang, A.J. Sinskey, H.F. Lodish, Oxidized redox state of glutathione in the endoplasmic-reticulum, *Science* 257 (5076) (1992) 1496–1502.
- [64] J.J. Hu, L.X. Dong, C.E. Outten, The redox environment in the mitochondrial intermembrane space is maintained separately from the cytosol and matrix, *J. Biol. Chem.* 283 (43) (2008) 29126–29134.
- [65] C.D. Austin, X.H. Wen, L. Gazzard, C. Nelson, R.H. Scheller, S.J. Scales, Oxidizing potential of endosomes and lysosomes limits intracellular cleavage of disulfide-based antibody-drug conjugates, *Proc. Natl. Acad. Sci. U.S.A.* 102 (50) (2005) 17987–17992.
- [66] V. Kodali, B.D. Thrall, *Oxidative Stress and Nanomaterial-Cellular Interactions*, Humana Press, 2015.
- [67] T. Zhang, M.J. Gaffrey, D.G. Thomas, T.J. Weber, B.M. Hess, K.K. Weitz, P. D. Piehowski, V.A. Petyuk, R.J. Moore, W.-J. Qian, B.D. Thrall, A proteome-wide assessment of the oxidative stress paradigm for metal and metal-oxide nanomaterials in human macrophages, *NanoImpact* 17 (2020) 100194.
- [68] K.M. Holmstrom, T. Finkel, Cellular mechanisms and physiological consequences of redox-dependent signalling, *Nat. Rev. Mol. Cell Biol.* 15 (6) (2014) 411–421.
- [69] N. Mesecke, A. Spang, M. Deponate, J.M. Herrmann, A novel group of glutaredoxins in the cis-Golgi critical for oxidative stress resistance, *Mol. Biol. Cell* 19 (6) (2008) 2673–2680.
- [70] R.J. Mailloux, Mitochondrial antioxidants and the maintenance of cellular hydrogen peroxide levels, *Oxid. Med. Cell Longev.* (2018), 7857251.
- [71] A. Rietsch, J. Beckwith, The genetics of disulfide bond metabolism, *Annu. Rev. Genet.* 32 (1998) 163–184.
- [72] T. Spector, T.E. Jones, R.L. Miller, Reaction mechanism and specificity of human GMP reductase. Substrates, inhibitors, activators, and inactivators, *J. Biol. Chem.* 254 (7) (1979) 2308–2315.
- [73] I. Dunand-Sauthier, C.A. Walker, J. Narasimhan, A.K. Pearce, R.C. Wek, T. C. Humphrey, Stress-activated protein kinase pathway functions to support protein synthesis and translational adaptation in response to environmental stress in fission yeast, *Eukaryot. Cell* 4 (11) (2005) 1785–1793.
- [74] D. Shenton, J.B. Smirnova, J.N. Selley, K. Carroll, S.J. Hubbard, G.D. Pavitt, M. P. Ashe, C.M. Grant, Global translational responses to oxidative stress impact upon multiple levels of protein synthesis, *J. Biol. Chem.* 281 (39) (2006) 29011–29021.
- [75] J.B. Smirnova, J.N. Selley, F. Sanchez-Cabo, K. Carroll, A.A. Eddy, J.E. G. McCarthy, S.J. Hubbard, G.D. Pavitt, C.M. Grant, M.P. Ashe, Global gene expression profiling reveals widespread yet distinctive translational responses to different eukaryotic translation initiation factor 2B-targeting stress pathways, *Mol. Cell Biol.* 25 (21) (2005) 9340–9349.
- [76] M. Ibba, D. Soll, Aminoacyl-tRNA synthesis, *Annu. Rev. Biochem.* 69 (2000) 617–650.
- [77] F.O. Martinez, L. Helming, S. Gordon, Alternative activation of macrophages: an immunologic functional perspective, *Annu. Rev. Immunol.* (2009) 451–483.
- [78] D. Fairweather, D. Cihakova, Alternatively activated macrophages in infection and autoimmunity, *J. Autoimmun.* 33 (3–4) (2009) 222–230.
- [79] A. Mantovani, P. Allavena, A. Sica, F. Balkwill, Cancer-related inflammation, *Nature* 454 (7203) (2008) 436–444.
- [80] B. Brune, N. Dehne, N. Grossmann, M. Jung, D. Namgaladze, T. Schmid, A. von Knethen, A. Weigert, Redox control of inflammation in macrophages, *Antioxidants Redox Signal.* 19 (6) (2013) 595–637.
- [81] D.N. Kekulandara, K.T. Samarasinghe, D.N. Munkanatta Godage, Y.H. Ahn, Clickable glutathione using tetrazine-alkene bioorthogonal chemistry for detecting protein glutathionylation, *Org. Biomol. Chem.* 14 (46) (2016) 10886–10893.
- [82] S. Feng, Y. Chen, F. Yang, L. Zhang, Y. Gong, G. Adilijiang, Y. Gao, H. Deng, Development of a clickable probe for profiling of protein glutathionylation in the central cellular metabolism of *E. coli* and *Drosophila*, *Chem. Biol.* 22 (11) (2015) 1461–1469.
- [83] M.D. Campbell, J. Duan, A.T. Samuelson, M.J. Gaffrey, G.E. Merrihew, J. D. Egerton, L. Wang, T.K. Bammler, R.J. Moore, C.C. White, T.J. Kavanagh, J. G. Voss, H.H. Szeto, P.S. Rabinovitch, M.J. MacCoss, W.J. Qian, D.J. Marcinek, Improving mitochondrial function with SS-31 reverses age-related redox stress and improves exercise tolerance in aged mice, *Free Radic. Biol. Med.* 134 (2019) 268–281.
- [84] D. Ezerina, B. Morgan, T.P. Dick, Imaging dynamic redox processes with genetically encoded probes, *J. Mol. Cell. Cardiol.* 73 (2014) 43–49.
- [85] R.M. Gill, M. O'Brien, A. Young, D. Gardiner, R.J. Mailloux, Protein S-glutathionylation lowers superoxide/hydrogen peroxide release from skeletal muscle mitochondria through modification of complex I and inhibition of pyruvate uptake, *PLoS One* 13 (2) (2018) e0192801–e0192801.
- [86] R.J. Mailloux, W.G. Willmore, S-glutathionylation reactions in mitochondrial function and disease, *Front. Cell Dev. Biol.* 2 (2014) 68.
- [87] K.T. Samarasinghe, D.N. Munkanatta Godage, Y. Zhou, F.T. Ndombera, E. Weerapana, Y.H. Ahn, A clickable glutathione approach for identification of protein glutathionylation in response to glucose metabolism, *Mol. Biosyst.* 12 (8) (2016) 2471–2480.
- [88] M. O'Brien, J. Chalker, L. Slade, D. Gardiner, R.J. Mailloux, Protein S-glutathionylation alters superoxide/hydrogen peroxide emission from pyruvate dehydrogenase complex, *Free Radic. Biol. Med.* 106 (2017) 302–314.